Characterization by Dilute Solution and Rheological Methods of Polystyrene and Poly(methyl methacrylate) Produced with a Tetrafunctional Peroxide Initiator

M. J. Scorah,[1] C. Tzoganakis,[1] R. Dhib,[2] A. Penlidis[1]

[1]*Institute for Polymer Research, Department of Chemical Engineering, University of Waterloo, Waterloo, Ontario N2L 3G1, Canada*
[2]*Department of Chemical Engineering, Ryerson University, Toronto, Ontario M5B 2K3, Canada*

Received 9 January 2006; accepted 13 July 2006
DOI 10.1002/app.25370
Published online in Wiley InterScience (www.interscience.wiley.com).

ABSTRACT: Polystyrene (PS) and poly(methyl methacrylate) (PMMA) samples produced by the bulk homopolymerization of styrene and methyl methacrylate with a tetrafunctional peroxide initiator (JWEB50) are characterized in detail by various solution and rheological methods. For comparison purposes, ''linear'' PS and PMMA samples were produced under similar conditions with a monofunctional initiator (TBEC). The four sample types were characterized by size exclusion chromatography (SEC) setups to determine molecular weight, radius of gyration, and intrinsic viscosity distributions. Contraction factors were calculated and indicated evidence of branching for polystyrene produced with JWEB50 while no such effects were observed with PMMA. The rheological behavior of the samples was subsequently investigated by performing oscillatory shear and creep experiments. Compared to the ''linear'' material, samples produced with JWEB50 exhibited a reduction in zero-shear viscosity that was attributed to long-chain branching. Retardation spectra were calculated based on creep data and converted to dynamic compliances that were then combined with the oscillatory data. This provided master curves spanning a much wider frequency range than could be obtained experimentally. Examination of various viscoelastic functions showed evidence of long-chain branching for both polystyrene and poly(methyl methacrylate) samples produced with JWEB50. © 2006 Wiley Periodicals, Inc. J Appl Polym Sci 103: 1340–1355, 2007

Key words: branching; rheology; size exclusion chromatography; solution properties; polystyrene; poly(methyl methacrylate)

INTRODUCTION

The characterization of branched polymers has been the focus of innumerable studies since their existence was postulated roughly 70 years ago.[1,2] Much of the fundamental understanding of branching and its influence on dilute solution and rheological properties began with specific molecular architectures such as stars and combs (see Refs. 3–7 for reviews). However, many commercially important polymers are produced by random polymerization processes and as such, have a distribution in both molecular weight and branching. This polydispersity in molecular weight and branching is the cause of difficulties in the characterization of such polymers and has led to a number of investigations on the detection of branching.[6,8-13]

Even today, the detection of long-chain branching (LCB) is considered as one of the most challenging and long standing problems in polymer science.[14] The importance of such a problem lies in the fact that these branched molecules can have a tremendous impact on the rheological properties even at extremely low concentrations. Spectroscopic and chemical methods relying on the differences in chemical structure that branching introduces, namely more end-groups or the existence of branch points, can be used to quantitatively determine the amount of branching without the need of a linear reference. The main limitation of these methods is that rarely are the differences between branch points or end-groups and normal repeat units significant enough to be detected for the very low concentrations of LCB that still influence the polymer's rheological properties.[8]

Similar to spectroscopic methods, chromatographic techniques, such as size exclusion chromatography (SEC), are widely used in the detection of LCB. It has been shown when examining the average solution properties of a polymer that the effects of branching can be masked by polydispersity. For this reason, fractionation methods in combination with various detectors are used to measure either the radius of gyration (R_g) or intrinsic viscosity ([η]) and in turn, allow the calculation of the corresponding contraction factors (g or g') as a function of molecular weight. Difficulties

Correspondence to: A. Penlidis (penlidis@uwaterloo.ca).
Contract grant sponsors: Natural Sciences and Engineering Research Council (NSERC), Canada; Canada Research Chair (CRC) Program.

Journal of Applied Polymer Science, Vol. 103, 1340–1355 (2007)
©2006 Wiley Periodicals, Inc.

can arise as some chromatographic techniques fractionate samples by hydrodynamic size and not molecular weight or branching. For example, in size exclusion chromatography, polymer molecules are separated based on hydrodynamic volume. In the case of a polydisperse sample having both molecular weight and branching distributions, it is possible for branched and linear molecules having identical hydrodynamic volumes but differing molecular weights to coelute.[11,15] Typically, the analysis of branched polymers with SEC assumes that the extent of branching increases with molecular weight because of the randomness of the polymerization reaction. As a result, partial separation of the branched chains does occur.

Because the flow behavior of polymers is tremendously susceptible to the presence of LCB, rheological methods are seen as the most sensitive and, in some instances, the last resort of detecting branching. A comprehensive method for the quantitative determination of LCB by rheological tests does not exist, as the degree, length, and structure of branching affect the rheological behavior of a polymer in various ways. The situation is even further complicated by variations in molecular weight distribution. In most studies, linear and branched materials are analyzed and a comparison of the linear viscoelastic properties, such as the zero-shear viscosity (η_0) or steady-state recoverable compliance (J_e^0), is used to provide evidence of branching. Others have attempted to quantify the degree of branching by various rheological indices or models.[14,16,17] Additional methods of detecting branching by rheological methods include the loss angle[18] or Van Gurp-Palmen plot,[19] thermorheological behavior,[17,20] and extensional rheology.[21,22] The dilemma with some of these test methods is that the absence of any difference between the behavior of linear and branched materials does not preclude the existence of branching. For example, higher values of the flow activation energies can be attributed to LCB. However, the reverse is not always true, as the presence of LCB does not necessarily enhance the activation energy.[17,23]

In previous studies, we have reported on the use of a tetrafunctional peroxide initiator (JWEB50) in the free-radical polymerization of styrene and methyl methacrylate (MMA).[24–26] The results of these investigations showed that higher rates of polymerization can be obtained with the tetrafunctional initiator compared to a monofunctional counterpart (TBEC) of similar thermal stability. However, the impact on molecular weight depends upon monomer type. With styrene, JWEB50 produced similar molecular weights to those obtained with TBEC, while for MMA, lower molecular weights compared to TBEC were measured. In this study, samples of polystyrene (PS) and poly (methyl methacrylate) (PMMA) produced with the tetrafunctional initiator, JWEB50, (PS-T and PMMA-T) and the monofunctional initiator, TBEC, (PS-M and PMMA-M) are characterized by SEC and rheological methods in an effort to detect evidence of branching.

EXPERIMENTAL

Materials

Polymer samples were produced from the bulk homopolymerization of styrene and methyl methacrylate initiated with a tetrafunctional peroxide initiator, JWEB50 (Atofina Chemicals, Philadelphia, PA). For comparison purposes, ''linear'' material was produced with a monofunctional initiator (*tert*-butylperoxy 2-ethylhexyl carbonate (TBEC), Atofina Chemicals). Details of the polymerization can be found elsewhere.[24–26]

Characterization

Size exclusion chromatography

Molecular weight, radius of gyration, and intrinsic viscosity distributions were measured using two size exclusion chromatography (SEC) setups. The first system was equipped with a multiangle laser light scattering (MALLS) detector (DAWN DSP, Wyatt Technology, Santa Barbara, CA), followed by a differential refractometer (2410 RI, Waters, Massachusetts, USA) in series. The second SEC employed Viscotek's quad detector comprised of a UV detector, low- (7°) and right-angle (90°) laser light scattering detectors (LALLS/RALLS), differential refractometer, and viscometer in series. The MALLS wavelength was 633 nm, while the laser wavelength of Viscotek's detector system was 670 nm. Although the specific refractive index increment (dn/dc) is a function of the laser wavelength, the difference between values at the two wavelengths was assumed to be negligible. Thus, dn/dc values of 0.185 mL/g and 0.083 mL/g were used for polystyrene (PS) and poly(methyl methacrylate) (PMMA). Analysis of data from the first SEC setup was performed with Astra v4.7 software (Wyatt Technology) and by selecting the Zimm method for analysis. Studies have found that the Zimm method or ''Inverse Debye method'' (plot of Kc/R_θ vs. $\sin^2(\theta/2)$) is linear over a much broader range of molecular weights, while other methods require increasing the order of the polynomial to better fit the light scattering data as the molecular weight increases throughout a sample.[13,27] For the second SEC setup, OmniSEC v3.0 (Viscotek, Houston, TX) software was employed in the analysis of data. In both situations, the second virial coefficient for the light-scattering equation was assumed to be negligible as very low concentrations of polymer were employed. Each SEC setup was equipped with one PLgel 10 μm guard column (50 × 7.5 mm^2) and three PLgel 10 μm MIXED-B columns (300 × 7.5 mm^2) (Polymer Laboratories, Amherst, MA). All columns and detectors were maintained at 30°C. Tetrahydrofu-

ran (THF) (Caledon Laboratories, Ontario, Canada) was filtered and used as the eluent at a flow rate of 1 mL/min. Polymer solutions of approximately 0.2 wt % were prepared and left for 12–24 h to fully dissolve. Injection volumes between 100 and 200 μL were used.

Differential scanning calorimetry

A Q100 differential scanning calorimetry (DSC) (TA Instruments, Delaware, USA) was used to measure the glass transition temperature, T_g, of polymer samples. Polymer samples (~10 mg) were sealed in aluminum pans and annealed at 200°C for 2 min. The samples were then cooled to 40°C and then scanned from 40 to 200°C at a heating rate of 10°C/min. Replicates of entire runs and scans showed good reproducibility of the data. The glass transition temperature was selected as the midpoint change in the heat capacity for the transition region.

Rheological testing

Oscillatory shear experiments and shear creep tests were performed to examine the viscoelastic behavior of polymer samples. Rheological data were collected using an AR2000 rheometer (TA Instruments) equipped with a parallel-plate geometry and an environmental test chamber for temperature control. All experiments were completed under a nitrogen atmosphere to avoid any degradation or crosslinking reactions. Sample discs (25 mm in diameter and 2.5 mm in thickness) were formed by compression molding roughly 1 g of polymer and 10 mg of antioxidant (Irganox 1010) at 190°C for several minutes. The linear viscoelastic region for each polymer was determined by conducting strain sweeps at 1 Hz. A series of strain-controlled frequency (ω) sweeps from 0.01 to 100 Hz were obtained for various temperatures in increments of 10°C for each sample. Frequency sweeps were then replicated with a new sample to ensure good reproducibility of results. In the case of PS, the temperature was varied from 160 to 220°C, while for PMMA, the range of 190–250°C was chosen. The upper temperature limits were selected to avoid the decomposition of polymer samples. To check whether degradation or crosslinking reactions occurred during the testing of samples, a frequency sweep at the lowest temperature was performed again. Good agreement with the original low temperature frequency sweep indicated that side reactions did not occur. As a second check, the molecular weight distributions of the samples after testing were determined by SEC and showed no evidence of degradation.

Creep experiments for PS and PMMA were conducted at 220 and 250°C, respectively. The linear viscoelastic region was determined by performing creep tests for a variety of shear stresses.[28] The limit of this region was established by comparing creep compliances ($J(t)$) for the various shear stresses and locating the stress where curves no longer coincided. For PS samples, the limit corresponded to a shear stress of 15 Pa while in the case of PMMA, a shear stress of 40 Pa was not exceeded.

RESULTS AND DISCUSSION

SEC-LS-viscometer

Compared to a linear chain of the same number of units, a branched chain is more compact. As a result, the impact of branching on the size of a polymer chain is to decrease the mean-square radius (S^2) as branching increases. To assess the decrease in size due to branching, the mean-square radius or radius of gyration (R_g) of a branched polymer is compared to the size of a linear analog of identical molecular weight. Quantitatively, this was defined by Zimm and Stockmayer[29] with the following branching or contraction factor:

$$g = \left.\frac{\langle s^2\rangle_{\mathrm{br}}}{\langle s^2\rangle_l}\right|_M = \left.\frac{R^2_{g\mathrm{br}}}{R^2_{gl}}\right|_M \tag{1}$$

The subscript M indicates that both the branched (br) and linear (l) chains have identical molecular weights. Because branched polymers are more compact and have smaller dimensions, g will always be less than unity with smaller values being an indication of a higher amount of branching. Theoretical equations for the calculation of contraction factors have been developed for various types of branched structures including stars,[29,30] combs,[31] and random branching.[29] For a monodisperse randomly branched polymer with trifunctional or tetrafunctional branch points, the contraction factors (g_3 and g_4) are given by:

$$g_3 = \left[\left(1+\frac{\overline{n}}{7}\right)^{1/2} + \frac{4\overline{n}}{9\pi}\right]^{-1/2} \tag{2}$$

$$g_4 = \left[\left(1+\frac{\overline{n}}{6}\right)^{1/2} + \frac{4\overline{n}}{3\pi}\right]^{-1/2} \tag{3}$$

where n̄ is the average number of branch points per chain. For polydisperse polymer samples, the weight–average contraction factors can be determined from the following:

$$\langle g_3\rangle_w = \frac{6}{n_w}\left[\frac{1}{2}\left(\frac{2+n_w}{n_w}\right)^{1/2}\ln\left(\frac{(2+n_w)^{1/2}+n_w^{1/2}}{(2+n_w)^{1/2}-n_w^{1/2}}\right)-1\right] \tag{4}$$

$$\langle g_4\rangle_w = \frac{1}{n_w}\ln(1+n_w) \tag{5}$$

TABLE I
Molecular Weight Characterization of Polystyrene and Poly(methyl methacrylate) Samples

	SEC-MALLS					SEC-LALS-Visc				
Sample	M_n (kg/mol)	M_w (kg/mol)	M_w/M_n	K_{R_g} (nm)	ν	M_n (kg/mol)	M_w (kg/mol)	M_w/M_n	$K_{[\eta]}$ (10^{-4} dL/g)	α
PS-M	312	582	1.9	0.0113	0.600	316	579	1.8	9.54	0.72
PS-T	264	628	2.4			282	629	2.2		
PMMA-M	455	854	1.9	0.0124	0.588	438	824	1.9	6.32	0.73
PMMA-T	471	844	1.8			456	803	1.8		

PS, polystyrene; PMMA, poly(methyl methacrylate); M, monofunctional initiator; T, tetrafunctional initiator.

where n_w is the weight–average number of branch points per chain. Although JWEB50 is a tetrafunctional initiator, it is possible for trifunctional branches to be generated. Various reactions in free-radical polymerizations can lead to such structures including transfer reactions and terminal double bond polymerization. In addition, it is possible that not all of the functional groups on a tetrafunctional initiator molecule will successfully generate a chain. As a result, it is plausible that 3-arm stars could be produced. It is for these reasons that equations for both tri- and tetrafunctional branch points are presented.

Comparable to eq. (1), a branching factor can be also defined using the intrinsic viscosity:

$$\left| g' = \frac{[\eta]_{\mathrm{br}}}{[\eta]_l} \right|_M \tag{6}$$

Because of the ease in measuring intrinsic viscosity relative to the radius of gyration, considerably more experimental work has reported intrinsic viscosity data for branched molecules.

Molecular weight averages and polydispersities for the PS and PMMA samples analyzed in this study are reported in Table I. The data are the average of two samples of each polymer injected twice. The results from the two SEC setups show good agreement. Figures 1 and 2 provide plots of radius of gyration and intrinsic viscosity for the PS and PMMA samples. The trends for PS show that, at higher molecular weights, PS-T has smaller values for the radius of gyration and intrinsic viscosity compared to PS-M. This observation indicates that PS-T is more branched than PS-M. Looking at Figure 2, radius of gyration and intrinsic viscosity plots do not show any differences be-

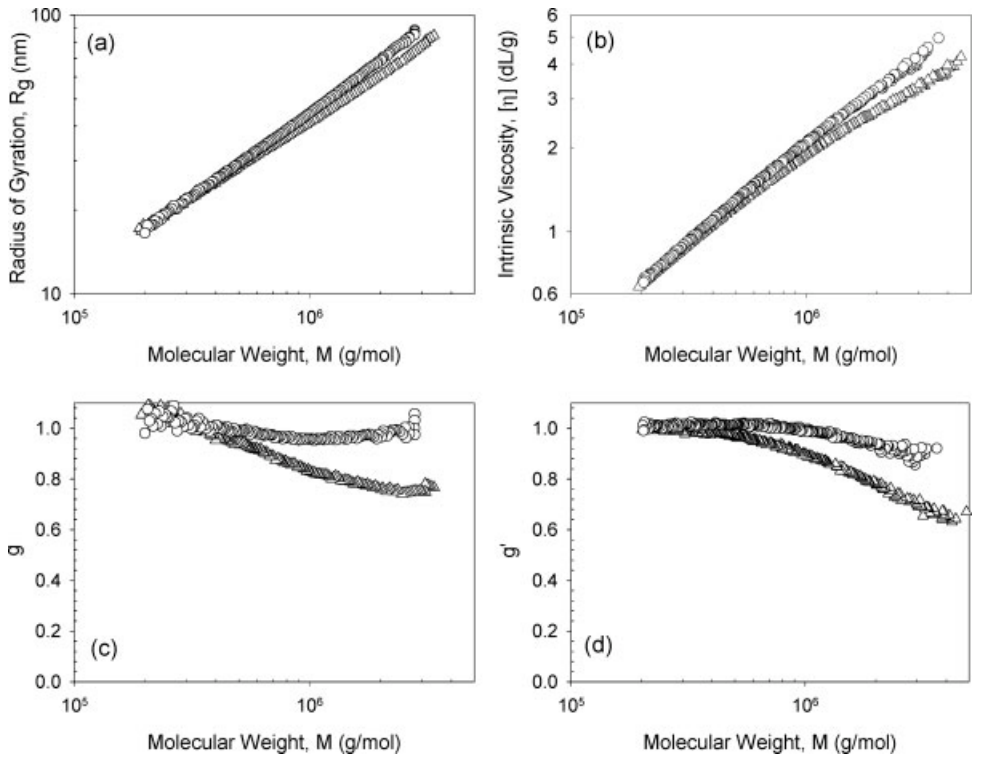

Figure 1 Plots of radius of gyration, intrinsic viscosity and their respective branching factors as a function of molecular weight for polystyrene samples (circles – PS-M; triangles – PS-T).

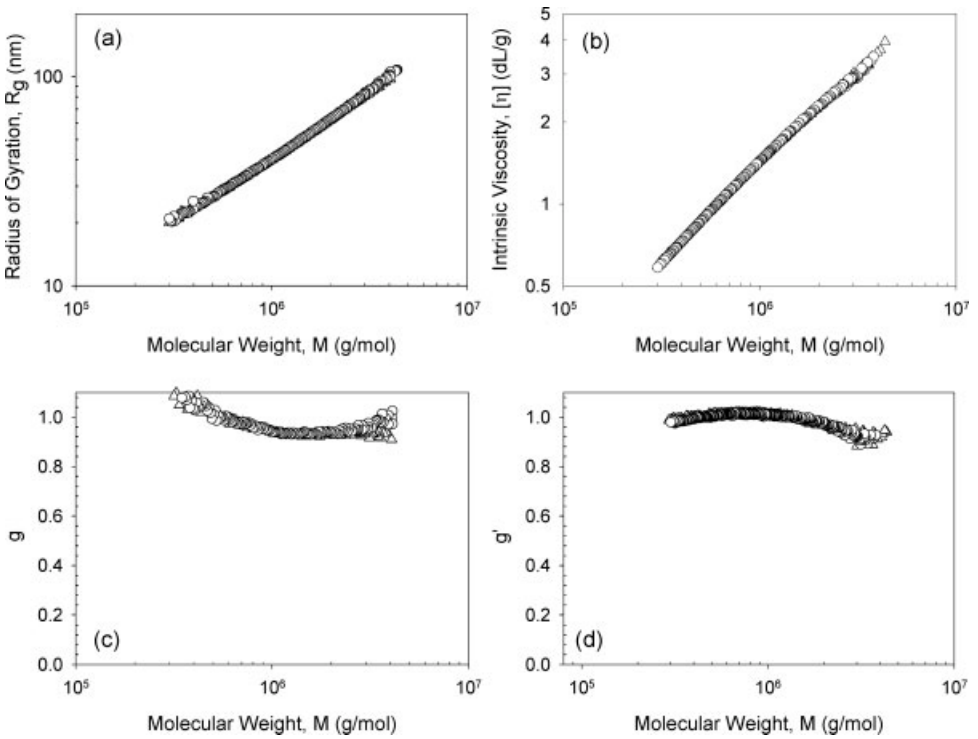

Figure 2 Plots of radius of gyration, intrinsic viscosity and their respective branching factors as a function of molecular weight for poly(methyl methacrylate) samples (circles – PMMA-M; triangles – PMMA-T).

tween PMMA samples. As such, there is no evidence of branching in PMMA-T compared to its corresponding M sample. The contraction factors for the radius of gyration (g) and intrinsic viscosity (g') are plotted in parts (c) and (d) of Figures 1 and 2. In the determination of the contraction factors, nonlinear regression was used to fit power-law models to the linear portion of $\log R_g - \log M$ and $\log [\eta] - \log M$ data of PS-M and PMMA-M based upon the following equations:

$$R_g = K_{R_g} M^v \tag{7}$$

$$[\eta] = K_{[\eta]} M^\alpha \tag{8}$$

where K_{R_g} and $K_{[\eta]}$ are the pre-exponential factors, and v and α are exponents. $k_{[\eta]}$ and α are also known as the Mark–Houwink (MH) constants. The estimated parameters are given in Table I and are similar to published values.[15,27,32,33] An interesting point to note is that the intrinsic viscosity plots for both PS-M and PMMA-M show some curvature near the high molecular weight end. Because of the random nature of free-radical polymerization, even with a monofunctional initiator, it is possible for branches to be formed via transfer reactions (even if at a very low level).

One of the difficulties in applying theoretical g equations to randomly branched polymers is the decision of what type of branching exists. In free-radical polymerization of monofunctional monomers, transfer reactions typically lead to trifunctional branch points. However, due to the structure of the tetrafunctional initiator, the presence of tetrafunctional branch points may be possible. The other dilemma that affects the choice of a proper equation is the assumption of whether samples fractionated by SEC are monodisperse or not. For example, coelution of branched and linear chains having the same hydrodynamic volume but differing molecular weight may occur and would result in a ''local'' polydispersity in the detector cell. In the published literature, there are examples of the use of both the monodisperse[34,35] and polydisperse equations for SEC data.[13,36]

Figure 3 is a plot of the number of long-chain branches as a function of molecular weight for PS-T. The data has been estimated from four cases: trifunctional versus tetrafunctional branching and monodisperse versus polydisperse fractions. All curves show the same trend of increasing number of LCB with increasing molecular weight. Estimates for the number of LCB are highest for trifunctional branching compared to tetrafunctional branching. For a particular molecular weight, a chain with trifunctional branch points requires more branch points per molecule to have a similar g value that a chain with tetrafunctional branching would have. Whether the SEC fractions were considered monodisperse or polydisperse also had a significant effect on the estimated number of branches per molecule. Fewer branches were predicted when using the equations for polydisperse fractions. Figure 4 provides a comparison of the number of long-chain branches for

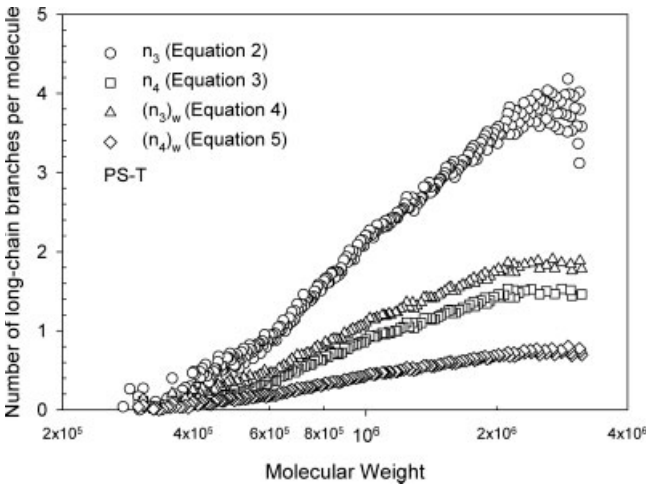

Figure 3 Number of long-chain branches per molecule as a function of molecular weight for PS-T. The subscript number denotes the type of branching (tri- or tetrafunctional), while the subscript w indicates a weight average.

PS-T and PS-M. To account for the possibility that the separation by SEC may not have been complete, equations assuming polydisperse fractions were used for the comparison. The data indicate that PS-M contains at most 0.25 and 0.10 branches per molecule assuming trifunctional and tetrafunctional branching, respectively. In the case of PS-T, the most highly branched (and highest molecular weight) fractions contain 1.8 and 0.80 branches, respectively. As PS-M was produced with a monofunctional initiator, it is unlikely these samples contain chains with tetrafunctional branching.

DSC

Glass transition temperatures are reported in Table II for the PS and PMMA samples. No significant difference exists between the samples produced with either initiator (within typical experimental errors). Except for highly branched structures where the ratio of chain ends to molecular weight becomes very high, the glass transition temperature of a branched polymer should be identical to that of its linear analog.[3] The T_g values reported in Table II agree well with those published in the literature for linear materials.[37]

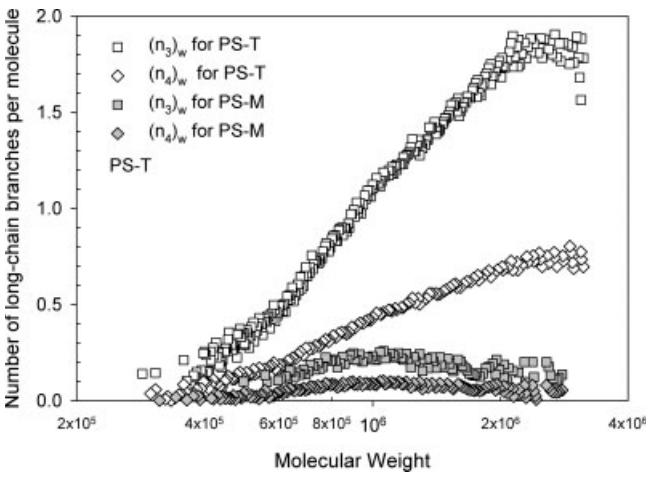

Figure 4 Number of long-chain branches per molecule as a function of molecular weight for PS-T and PS-M samples. The subscript number denotes the type of branching (tri- or tetrafunctional) while the subscript w indicates a weight average.

TABLE II
Material Properties for Polystyrene and Poly(methyl methacrylate) Samples

Sample	T_g (°C)	η_0 (kPa s)	J_e^0 (1/Pa)	G_N^0 (10^5 Pa)	τ_{0n} (s)	τ_{0w} (s)
PS-M	107	55	9.2×10^{-3}	1.8	0.29	510
PS-T	105	14	1.6×10^{-2}	1.5	0.097	240
PMMA-M	124	1340	1.7×10^{-4}	2.7	5.0	230
PMMA-T	124	708	1.4×10^{-4}	2.8	2.5	100

T_{ref} for PS is 220°C and 250°C for PMMA.

Rheological testing

Oscillatory shear experiments

Using the principles of time–temperature superposition (TTS), curves for viscoelastic properties at several temperatures were combined to form a single master curve by shifting the data horizontally (frequency axis) and vertically (modulus axis). Horizontal and vertical shift factors were determined according to the methods described by Mavridis and Shroff.[38]

Horizontal shift factors (a_T) for the samples analyzed in this study are plotted in Figure 5. The reference temperature was arbitrarily chosen as the maximum measurement temperature for the two sets of samples (220°C for PS and 250°C for PMMA). For each polymer sample, oscillatory shear experiments were replicated with a new sample disc. In the case of PS, the replicated data agrees well, showing good reproducibility for these measurements. Looking at the data for the PMMA samples, the agreement is not quite as good but still adequate.

One of the earliest models to predict horizontal shift factors as a function of temperature is the Williams-Landel-Ferry (WLF) equation:

$$\log a_T = \frac{-c_1(T - T_0)}{c_2 + T - T_0} \tag{9}$$

where c_1 and c_2 are WLF parameters for the reference temperature T_0. Although introduced as an empirical expression, the physical significance of the WLF equation is described by Ferry.[39] The WLF equation has been found to be valid for temperatures near the glass transition temperature, from T_g to $T_g + 100$°C. Above these temperatures and for relatively narrow tempera-

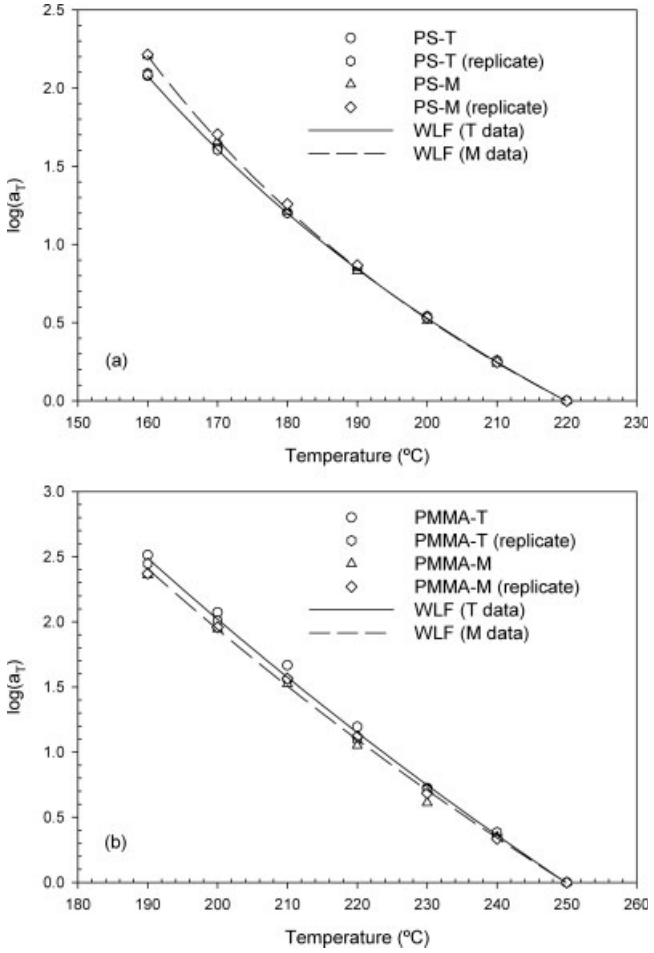

Figure 5 Logarithm of horizontal shift factors as a function of temperature for polystyrene and poly(methyl methacrylate) samples.

ture ranges, horizontal shift factors are typically fit to an ''Arrhenius'' type model:

$$a_T = \exp\left(\frac{E_a}{R}\left(\frac{1}{T} - \frac{1}{T_0}\right)\right) \tag{10}$$

where E_a is referred to as the activation energy for flow. The WLF equation was fit to the experimental horizontal shift factors and the parameter estimates are reported in Table III. 95% joint probability contour regions (JCR) are shown for the WLF parameters in Figures 6 and 7.

When looking at the horizontal shift factors for the PS samples, PS-T and PS-M have similar a_T values

TABLE III
Model Parameters for Horizontal Shift Factors

Sample	c_1	C_2 (K)	T_0 (K)	Horizontal E_a (kJ/mol)
PS-M	3.7	160	493	140 ± 6
PS-T	4.5	191	493	136 ± 4
PMMA-M	12.6	373	523	183 ± 3
PMMA-T	15.8	441	523	192 ± 3

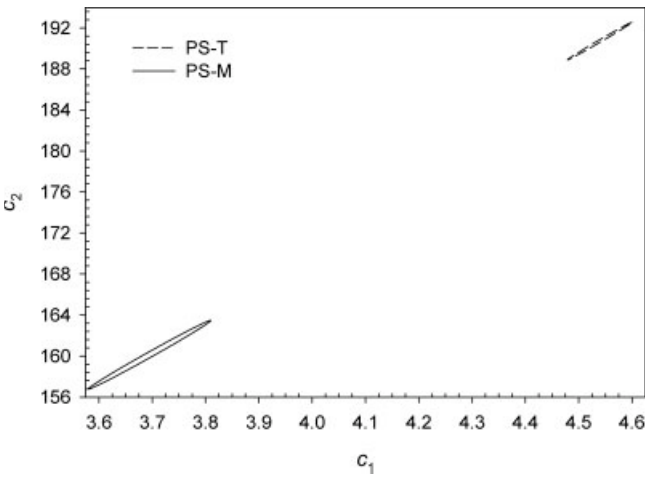

Figure 6 95% Joint probability contour regions for WLF parameters estimated from polystyrene data.

close to the reference temperature of 220°C [Fig. 5(a)]. However, for lower temperatures, a noticeable difference can be seen between the two sets of data as the PS-M data require larger horizontal shift factors compared to PS-T. This divergence leads to different estimates of the WLF parameters for the two sets of PS data. The 95% joint probability contour plots indicate that the estimates from the two sets of data are statistically different as no parts of the contour regions overlap (Fig. 6). For the PMMA samples, the horizontal shift data in Figure 5(b) indicates that there is a slight difference between the results for PMMA-M and PMMA-T and different WLF constants are estimated for each sample. The JCR plots in Figure 7 show that there is more uncertainty in the parameter estimates for the PMMA samples compared to the PS samples. This was expected as there is more scatter in the PMMA data. The joint probability contour regions for the WLF parameters of PMMA-M and PMMA-T,

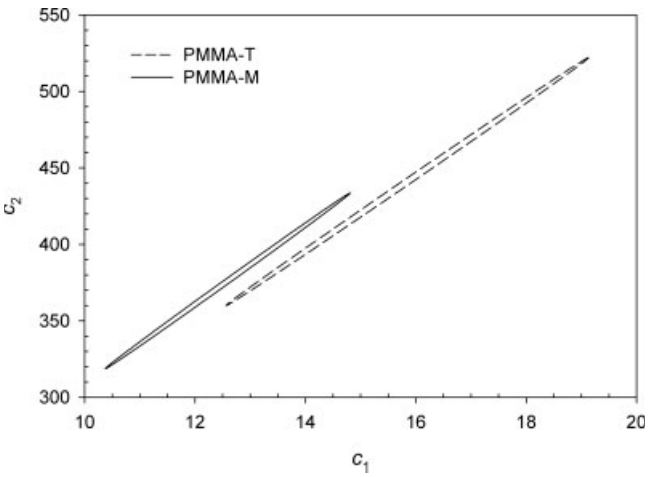

Figure 7 95% Joint probability contour regions for WLF parameters estimated from poly(methyl methacrylate) data.

however, are quite close. The difficulty in dealing with the WLF equation is that the parameters are highly correlated, shown by the (elliptical) contours that almost approach the shape of a line. As a result, any increase (or decrease) in c_1, must be followed by an increase (or decrease) in c_2 and vice versa.

The ''Arrhenius'' model given in eq. (10) was also fit to the horizontal shift factors. The horizontal activation energies and a 95% confidence interval are given in Table III while the model fits are shown in plots of $\log(a_T)$ as a function of $1/T$ (Fig. 8). For the PS samples, the 95% confidence intervals of the activation energies were found to overlap and thus, would indicate that there is no statistical difference between the two sets of data. When looking at the model predictions for PS-M and PS-T in Figure 8(a), it can be seen that there are indications of a model lack of fit. In a plot of $\log(a_T)$ vs. $1/T$, each of the PS data sets has some curvature that an ''Arrhenius'' model cannot account for. Although not shown here, plots of the residual error versus $1/T$ showed a parabolic shape, which also provided evidence of lack of fit. These results along with the fact that the sum of squared residuals is lower for the WLF model compared to the ''Arrhenius'' model indicate that the WLF equation is better suited for the PS data. This can be reasoned based on the fact that the WLF equation has been found to be valid between T_g and $T_g + 100°C$. For PS-M and PS-T, this range would encompass ~105–207°C. Apart from the highest temperature of 220°C, the PS data were collected within this interval. The ''Arrhenius'' model has been found to provide a better fit for temperatures above $T_g + 100°C$. In contrast to the trends found with PS, the activation energies for PMMA did show a statistical difference where PMMA-T was found to have a higher E_a value. Model predictions using the ''Arrhenius'' model agreed well with the experimental PMMA data, which in this case did not show curvature in plots of $\log(a_T)$ versus $1/T$ [Fig. 8(b)]. The ''Arrhenius'' model performed better with the PMMA data compared to the PS data, because more of the PMMA data was collected outside the range of the WLF equation's applicability.

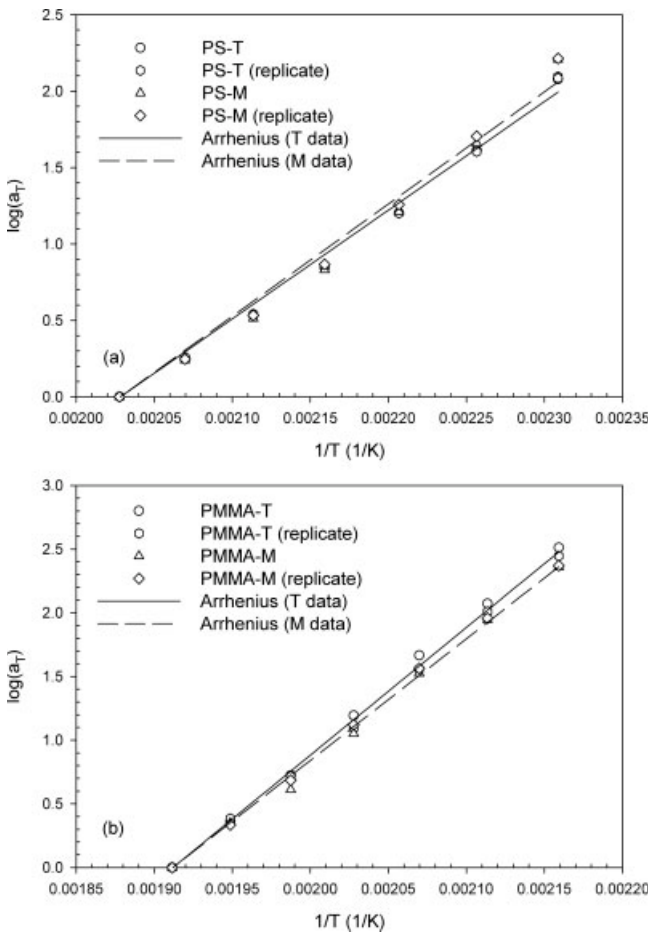

Figure 8 Logarithm of horizontal shift factors as a function of inverse temperature for polystyrene and poly(methyl methacrylate) samples.

The relationship between branching and the horizontal activation energy is not well known. It is generally accepted that a higher activation energy can be attributed to LCB; however, the presence of LCB does not always lead to an enhancement in E_a. As such, activation energies estimated for the PMMA samples, indicate that PMMA-T is more branched than PMMA-M. PS samples showed no differences in their E_a estimates, and thus, it cannot be stated from this method whether PS-T or PS-M is more branched. This is in contrast to the results found from SEC where a difference between samples was detected with PS and not with PMMA.

Although not reported here,[40] plots of the vertical shift factor (b_T) did not show any significant differences when comparing PS-T to PS-M and PMMA-T to PMMA-M. According to the Rouse model, the vertical shift factor is related to temperature by the following[41]:

$$b_T = \frac{\rho_0 T_0}{\rho T} \tag{11}$$

where ρ_0 and ρ are the polymer densities at temperatures T_0 and T. Vertical shift factors generated from the above equation do not work well for every polymer but a more general equation is not available.[20,42] Neither eq. (11) nor an ''Arrhenius'' model could adequately fit the b_T data as both models showed a significant lack of fit.

The fact that smooth master curves could be generated for various viscoelastic functions (Figs. 9 and 10) and that horizontal shift factors followed the WLF equation indicates that the application of TTS for the samples studied is valid. Therefore, no evidence of thermorheological complexity was observed. Storage and loss moduli (G', G'') master curves are plotted in Figures 9 and 10. In the case of PS, curves for PS-T

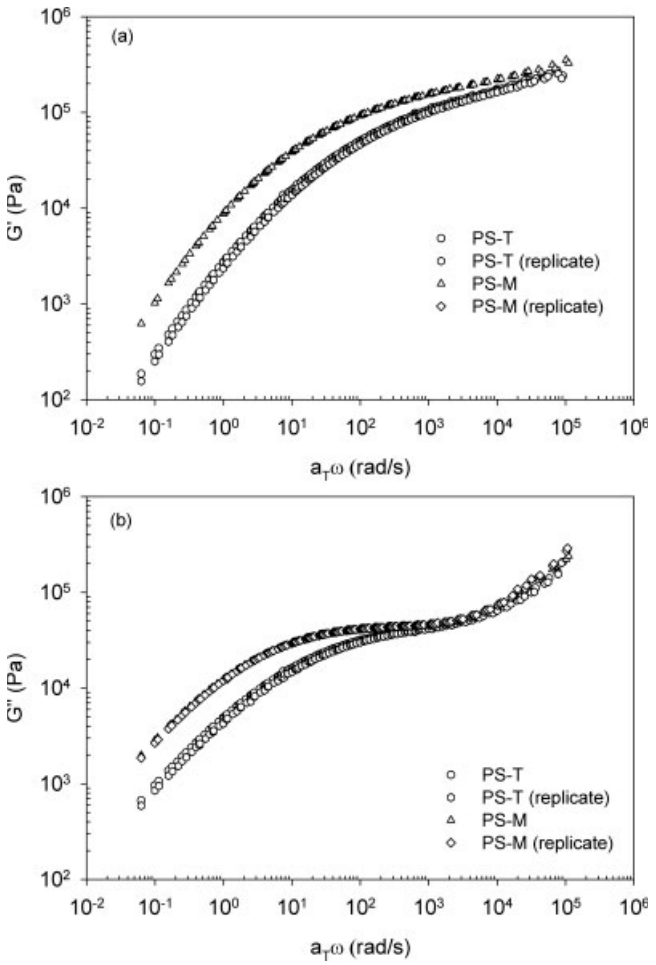

Figure 9 Storage and loss moduli master curves at 220°C for polystyrene samples.

and PS-M show distinct differences. Because many factors such as molecular weight, polydispersity, and branching influence the storage and loss moduli curves, it is difficult to assign a divergence between curves to any one factor. When examining the master curves for the PMMA data (Fig. 10), very little difference can be seen between samples PMMA-T and PMMA-M. For the storage modulus, both curves have the same shape, except that the data for PMMA-T is slightly lower in the low frequency range. In the case of the loss modulus, it is difficult to discern any difference between the two samples due to the scatter in the data. However, similar to the storage modulus, PMMA-T moduli are lower than PMMA-M at the very low frequency range.

The zero-shear viscosity and steady-state recoverable compliance can be calculated from dynamic moduli obtained in the terminal region (low frequency). In the case of the PS samples, the dynamic data only just reaches the terminal zone, while data for PMMA does not. To obtain data in the terminal region, either lower frequencies or higher temperatures would be needed. Lower frequencies could not be readily achieved due to the limits of the experimental apparatus. Running the samples at higher temperatures was also not possible due to the likelihood of thermal degradation. Between 200 and 300°C, the thermal degradation of unstabilized PS generates a decrease in molecular weight while volatile products are not produced until temperatures above 300°C are reached.[43] For unstabilized PMMA, minor thermal degradation begins as early as 165°C with the scission of head-to-head linkages followed by two major steps of degradation at 270 and 350°C.[44] Stabilization of PMMA almost completely reduces the effect of the first and second degradation steps but has no effect on the third.[45] There is a third option to obtain curves over a wider range of frequencies. Because linear viscoelastic functions are interrelated, data from various experimental tests can be combined to generate curves that span a greater frequency range. Thus, creep tests were performed and the viscoelastic functions were converted to dynamic data.

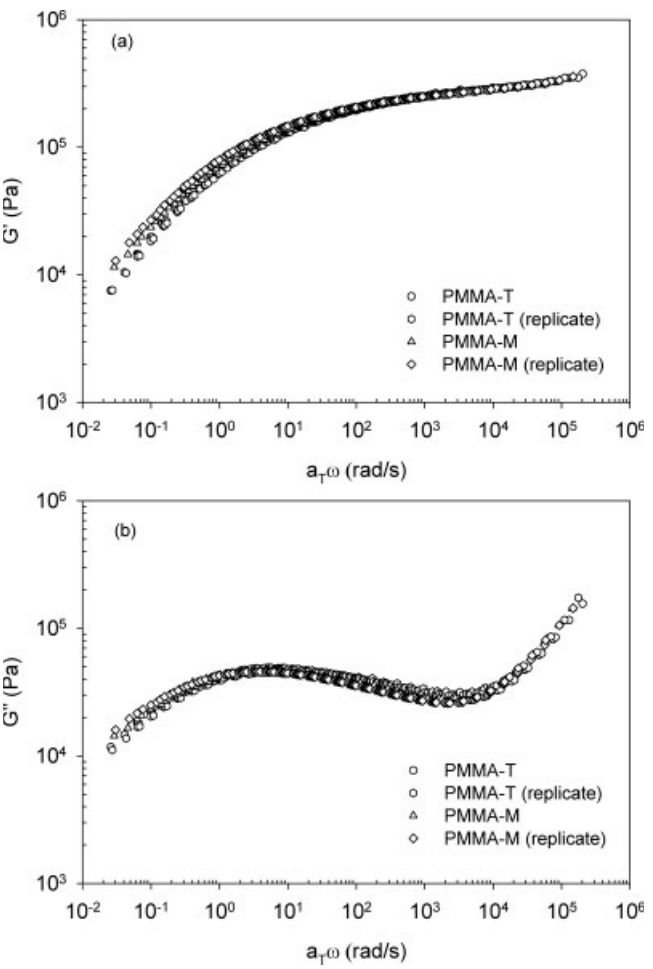

Figure 10 Storage and loss moduli master curves at 250°C for poly(methyl methacrylate) samples.

Shear creep experiments

Creep experiments were replicated three times and showed good agreement. The results of these experiments are shown in Figure 11. Note that for both PS and PMMA, the M series has compliances lower than their corresponding T sample. Molecular weight, polydispersity, and branching are all factors that influence the shear creep compliance. Because the PMMA samples have fairly similar molecular weight averages and polydispersities, the difference between compliance curves can be attributed to the effect of branching. However, in the comparison of PS samples, there is a slight difference in molecular weight averages and polydispersity that prevents attributing the difference in trends solely to the effect of branching.

The zero-shear viscosity (η_0) and steady-state recoverable compliance (J_e^0) were determined from the creep data and are reported in Table II. For both types of polymer, the T series has a lower zero-shear viscosity compared to the M series samples. The effect of LCB on the zero-shear viscosity depends upon the type and length of branching and both reductions and enhancements in η_0 have been observed. The introduction of branching leads to a decrease in a polymer's molecular size, and in turn, fewer molecular entanglements. However, when the branch length is sufficiently long, the overall number of entanglements will increase. Assuming that the general trend for linear polymers applies in that the zero-shear viscosity scales with molecular weight to the power of 3.4, the difference in molecular weight (MW) for the samples analyzed will not significantly affect η_0 ($\eta_{0T}/\ \eta_{0M}$ $(MW_T/MW_M)^{3.4}$: for PS, ratio = 1.3 and for PMMA, ratio = 0.92). Any differences in polydispersity can also be disregarded as the molecular weight distribution does not have a major influence on zero-shear viscosity.[34] Thus, the results indicate that both PS-T and PMMA-T are more branched than their corresponding M samples.

When examining the steady-state recoverable compliance (J_e^0) data, there is not such an obvious trend. The PS-T sample exhibits a much larger elasticity compared to PS-M, while the steady-state recoverable compliance of PMMA-T is lower than the value for PMMA-M. Similar to the effect of LCB on zero-shear viscosity, the presence of branching can either increase or decrease (J_e^0). When looking at the results in Table II, it is difficult to state a definite conclusion because the steady-state recoverable compliance is also highly sensitive to polydispersity, especially to small amounts of very high molecular weight material.[16,46] A broader molecular weight distribution produces a much higher (J_e^0).[46]

Chromatograms of PS-T showed a high molecular weight fraction that led to a larger polydispersity compared to PS-M. From the results, it appears that the high molecular weight fraction led to a larger value of the steady-state shear compliance and masked any effects of LCB. A similar trend was observed for PMMA. PMMA-M has a broader molecular weight distribution and a slightly larger (J_e^0) compared to PMMA-T.

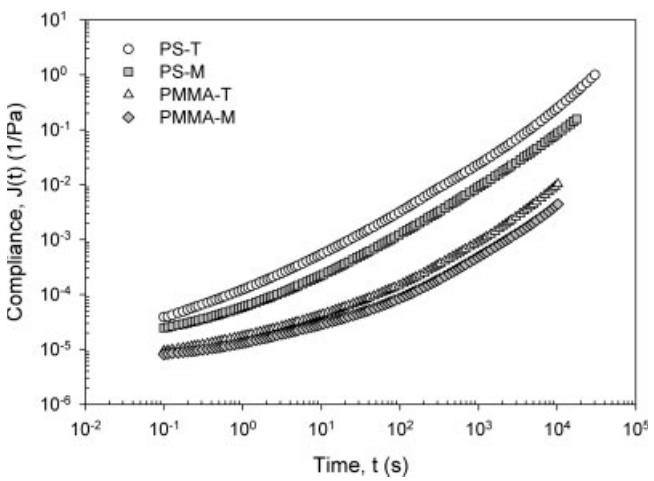

Figure 11 Shear creep compliance versus time for polystyrene samples at 220°C and poly(methyl methacrylate) samples at 250°C.

Combining dynamic and creep viscoelastic data

Theoretically, viscoelastic data obtained from one type of experiment can be converted into another. For example, it is possible to take time-dependent creep data, convert it to frequency-dependent data and thus, obtain viscoelastic functions over a wider frequency range. The general equations that relate the stress relaxation modulus $G(t)$, storage modulus $G'(\omega)$, loss modulus $G''(\omega)$, creep compliance $J(t)$, storage compliance $J'(\omega)$, loss compliance $J''(\omega)$, continuous relaxation spectrum $H(\tau)$, and continuous retardation spectrum $L(\tau)$ can be found in various texts.[39] The determination of either the relaxation or retardation spectrum from measurable viscoelastic data requires the inversion of a Fredholm integral equation of the first kind and is known as an ill-posed problem.[47] A software program (NLREG, Freiburg Materials Research Center, Albert-Ludwigs University of Freiburg, Germany) using a nonlinear Tikhonov regularization method has been developed to solve this problem.[48]

Utilizing NLREG, creep data in the form of $J(t)$ were used to determine the retardation spectrum for each of the samples. This spectrum was then employed to generate the compliance estimates as a function of frequency from which other viscoelastic functions could easily be determined. Figure 12 shows the complex compliance (J^*) data generated by the conversion of the creep time-dependent data to frequency-dependent data. The results from the dynamic testing are also plotted. The two types of data coincide well in the mid-

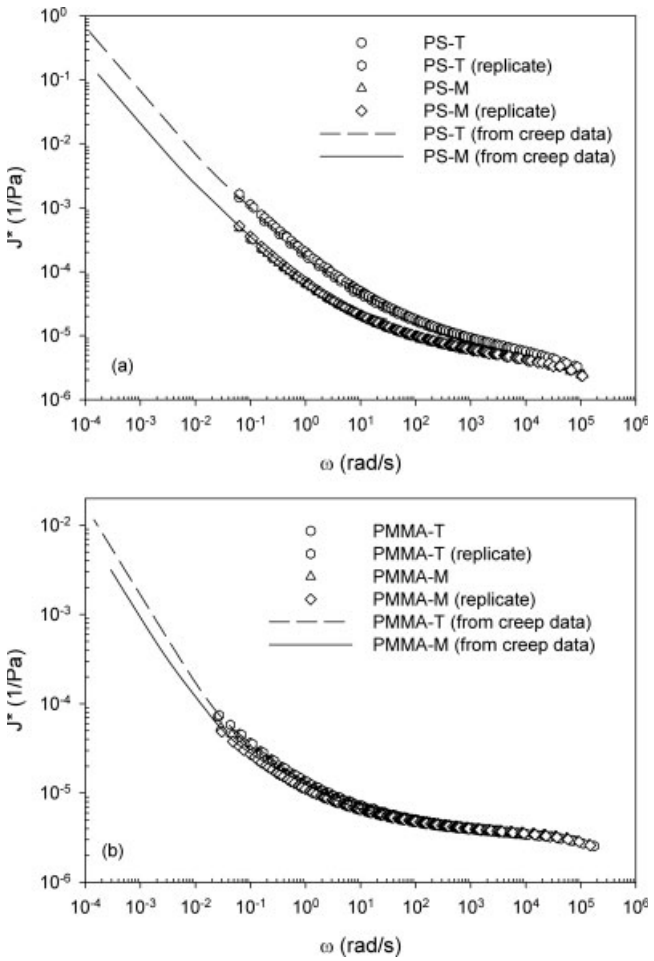

Figure 12 Complex compliance as a function of frequency for polystyrene samples at 220°C and poly(methyl methacrylate) samples at 250°C. Data points are master curves obtained from dynamic experiments while lines were generated by converted creep data.

frequency range ($0.02 < \omega < 30$ rad/s), where the converted data (lines) overlaps the dynamic data (points). Combining the two data sets has now extended the frequency range by at least two decades. More importantly, it has provided data in the terminal region that was otherwise difficult to obtain with dynamic testing. For the PS samples, the dynamic data was already sufficient enough to detect differences in the behavior of PS-T compared to PS-M. However, upon examination of the dynamic data for the set of PMMA samples, only a slight divergence between curves can be seen in the low frequency range ($0.02 < \omega < 0.1$ rad/s). With the aid of the converted creep data, the difference in complex compliance curves is much more obvious. Plots of the storage and loss modulus master curves based on the combination of dynamic and creep data for the PS and PMMA samples are shown in Figure 13. Differences between the PMMA samples are more apparent compared to plots of just the dynamic data (compare with Fig. 10).

Relaxation spectrum

Storage and loss modulus data generated by the combination of dynamic and creep data shown in Figure 13 were used to determine relaxation spectra with the computer program NLREG. The results are plotted in Figure 14 in the form of the relaxation strength as a function of relaxation time. The relaxation spectra are valid in a range of relaxation times corresponding to $\tau_{min} = (\omega_{max})^{-1}$ and $\tau_{max} = (\omega_{min})^{-1}$, where ω_{max} and ω_{min} are the maximum and minimum frequencies of the dynamic data.[46] The shape of the spectra is comparable to expected trends for polymers with broad molecular weight distributions.[39] At very small relaxation times, the relaxation strength is fairly large and decreases quickly during the transition zone. In the midrelaxation region, H is relatively flat while in the terminal region, the relaxation strength approaches zero. Polymers of narrow molecular weight distribution show a well-defined sharp decrease in H in the terminal region while polydisperse polymers exhibit a less abrupt drop in the relaxation strength. Examining the relaxation spectra for the PS samples, it can be seen that in the midrange of relaxation times ($10^{-5} < \tau < 10^{-3}$), the two samples have similar relaxation strengths. For very low relaxation times ($\tau < 10^{-5}$), there may be a significant divergence between the curves; however, this is outside the range of validity of the relaxation spectrum ($\tau_{min} = 1/\omega_{max} = 10^{-5}$). The maxima observed at the short-time end of the spectrum for PS-M and other undulations can be attributed to experimental scatter and numerical artifacts.[49] At times, the NLREG program attempts to fit the experimental data exactly, but at the expense of introducing meaningless maxima and minima. As a solution, the number of experimental data points used in the creep conversion process was reduced and the number of relaxation times calculated was kept to 10 points per decade. Both steps were found to considerably reduce the undulations in the relaxation spectra. Significant differences between the relaxation spectrum of PS-T and PS-M can be seen from the mid relaxation times onwards. The curve for PS-T begins to decrease at shorter times than PS-M and corresponds to PS-T having a lower zero-shear viscosity. Relaxation spectra for PMMA-T and PMMA-M are shown in Figure 14(b). The curves show the same general trend where H decreases sharply into a slight minimum and then drops to zero in the terminal region. Both samples have similar spectra until the terminal region is reached where the relaxation strength of PMMA-T begins to drop at a smaller relaxation time. Because the samples analyzed in this study have broad molecular weight distributions, the onset of the terminal region is not sharply defined and a terminal relaxation time is not easily identified. However, other measures of the relaxation spectrum

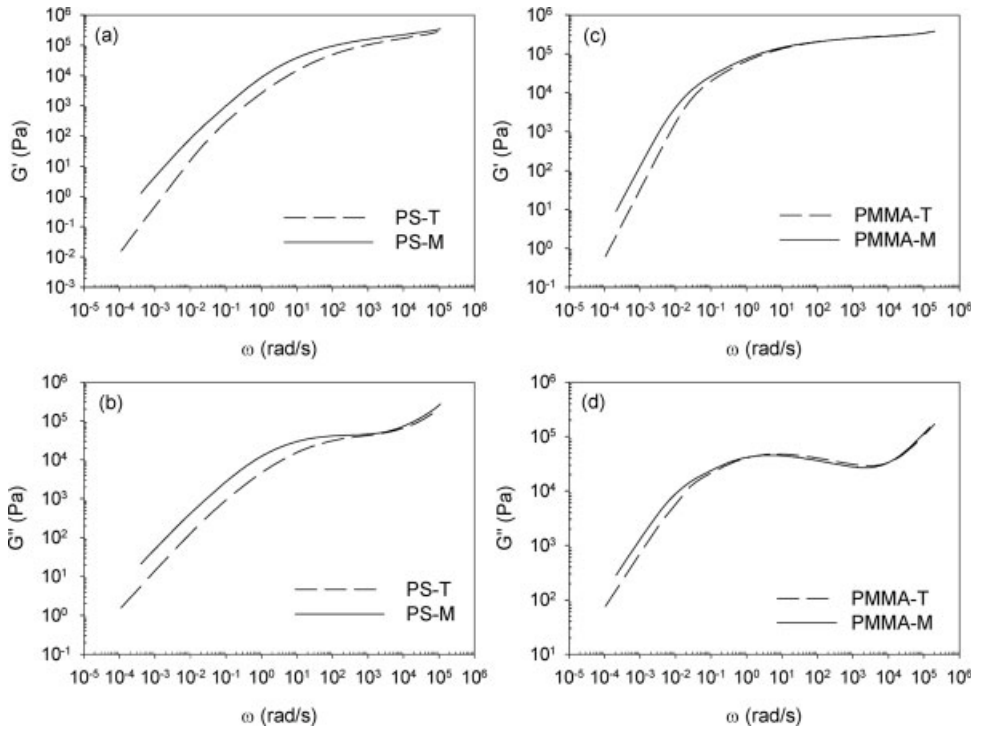

Figure 13 Storage and loss modulus master curves generated by combining dynamic and creep data for polystyrene at 220°C and poly(methyl methacrylate) at 250°C.

can be defined such as the number– and weight–average terminal (longest) relaxation times:

$$\tau_{0n} = \frac{\eta_0}{G_N^0} \tag{12}$$

$$\tau_{0w} = \eta_0 J_e^0 \tag{13}$$

where G_N^0 is the plateau modulus. Estimates of τ_{0n} and τ_{0w} are given in Table II. Both PS-M and PMMA-M show much higher values of the number– and weight–average terminal relaxation times. Since branching in PS-T and PMMA-T has been found to significantly reduce η_0, this has produced lower terminal relaxation times.

Viscosity

When investigating dynamic and steady-flow viscosity measurements, Cox and Merz[50] observed that curves of viscosity as a function of shear rate overlapped complex viscosity versus frequency data. Their empirical correlation was expressed as:

$$\eta(\dot{\gamma}) = |\eta^*(\omega)| \tag{14}$$

where $[\dot{\gamma}]$ is the shear rate and η^* is the complex viscosity. More often than not, viscoelastic data is collected in the linear region, typically due to the ease of running such experiments; however, the processing of polymers is typically performed in the nonlinear region. Use of the Cox-Merz correlation allows data from the linear region to be used in the study of nonlinear viscoelastic behavior. The application of this empirical rule has been found to be valid for several polymers including those containing branched chains.[51] Assuming that it can be used for the polymers analyzed in this study, viscosity-shear rate relations can be fit to the experimental data. Figure 15 is a log–log plot of viscosity as a function of shear rate for the samples analyzed in this study. The generalized Cross-Carreau model was fit to the experimental data:

$$\eta = \frac{\eta_0}{\left(1 + \left(\frac{\eta_0 \dot{\gamma}}{\tau^*}\right)^a\right)^{\frac{1-n}{a}}} \tag{15}$$

where τ^*, a, and n are the unique parameters of a polymer sample. τ^* characterizes the shear-stress level at which the viscosity transitions between the two asymptotic limits (Newtonian and power-law regions). n corresponds to the power-law index while a allows the model to better fit the transition region and characterizes the breadth between the two limiting behaviors. The Cross model corresponds to $a = 1 - n$ and allows for a broad transition region while the Carreau model uses $a = 2$ which produces a much narrower transition. From the different model types regressed to the data, both the Carreau and Cross models showed a lack of fit and as such, the

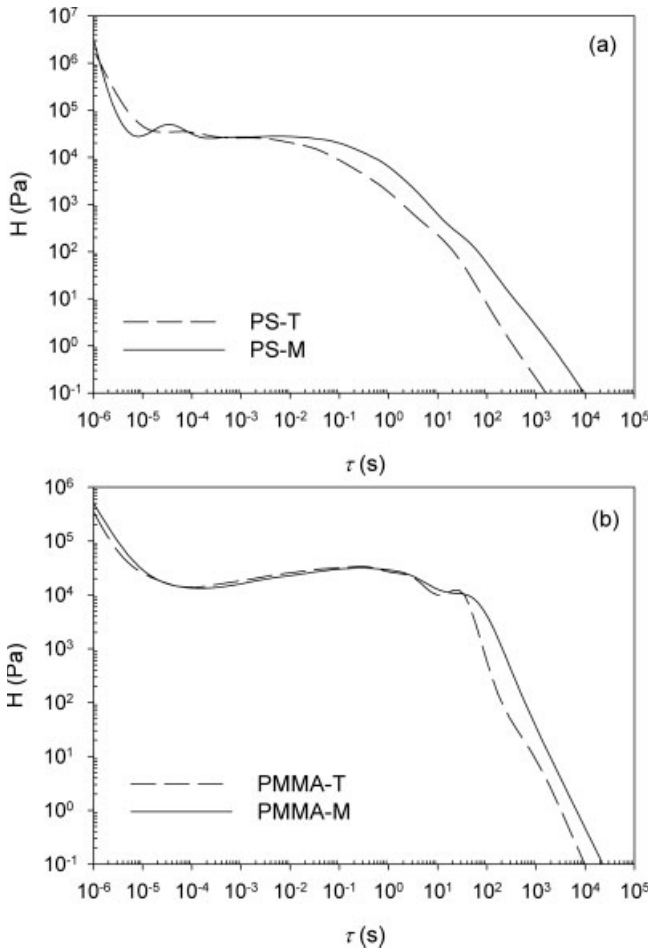

Figure 14 Relaxation spectra for polystyrene and poly (methyl methacrylate) samples.

results are not reported. The generalized Cross-Carreau model performed much better than the other models and the predictions are shown in Figure 15. Parameter estimates for the PS and PMMA samples are reported in Table IV. Although not shown here, joint probability contour regions were examined for the various parameter estimates and found to be extremely small and more circular in shape than elliptical. The latter finding indicates that the parameter estimates are not highly correlated. Comparison of JCR plots within polymer type showed no overlap at a significance level of 95%, indicating that there exists a significant statistical difference between parameter estimates of PS-T versus PS-M and PMMA-T versus PMMA-M. Estimates of the zero-shear viscosity from the Cross-Carreau model are similar to the values obtained from creep data (Table II) and show the same trend where samples PS-T and PMMA-T have lower values of η_0 compared to their corresponding M samples. When examining estimates of τ^*, it appears that the transition between the Newtonian and power-law regions occurs at lower shear-stress levels for the T series of samples. However, it is difficult to directly compare values of τ^* as samples have varying zero-shear viscosities. A characteristic time for this transition can be defined as the ratio of η_0/τ^*. It can be seen from the ratios listed in Table IV that the T samples have a lower characteristic time for the transition to shear thinning. In terms of the data plotted in Figure 15, this result implies that the onset of shear thinning occurs at higher shear rates for the T samples. As well, PS-T and PMMA-T have higher values of the exponent n indicates less shear thinning. Differences in the viscosity profile of each sample are more clearly observed by plotting a reduced viscosity (η/η_0) versus shear rate as presented in Figure 16. Curves for PS-T and PMMA-T begin to deviate from unity at higher shear rates and exhibit less of a dependence on shear rate in the power-law region compared to their M counterparts.

The shift in the transition region to higher shear rates has been attributed to LCB.[52,53] It has been reasoned that for relatively short branches or high branching densities, the probability of chain entanglement is

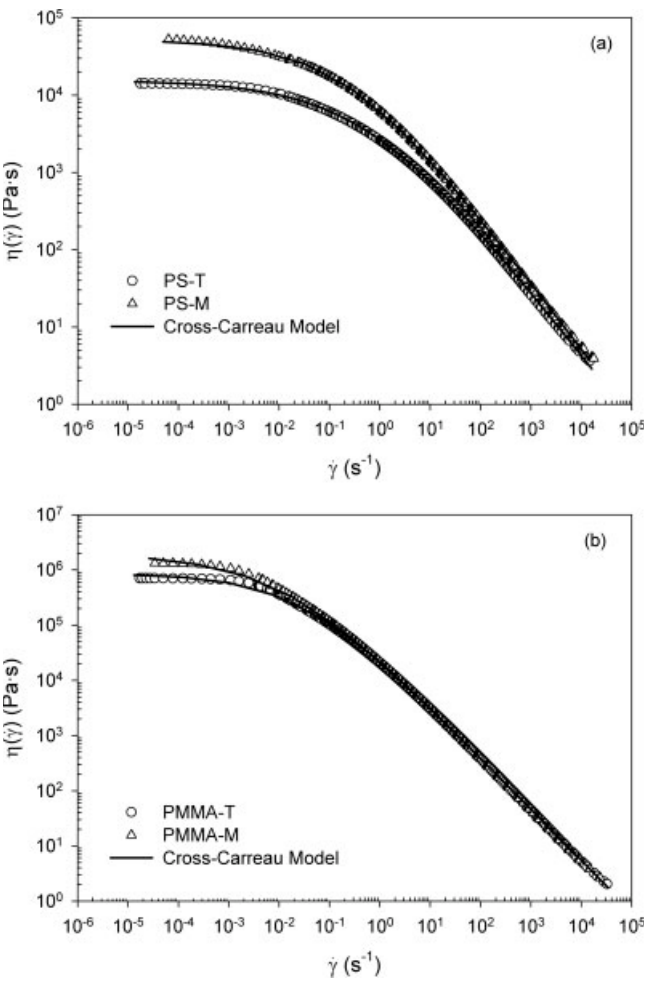

Figure 15 Viscosity versus shear rate for polystyrene and poly(methyl methacrylate) samples. Parameters for the Cross-Carreau model are given in Table IV.

TABLE IV
Cross-Carreau Model Parameters

Sample	η_0 (kPa s)	τ^* (kPa)	a	n	η_0/τ^* (s)
PS-M	51.3	11.9	0.433	0.139	4.31
PS-T	15.4	9.27	0.377	0.162	1.66
PMMA-M	1920	24.9	0.407	0.0551	77.1
PMMA-T	850	22.3	0.476	0.0700	38.1

reduced because of a branched chain's smaller molecular size. A linear polymer of similar molecular weight but greater molecular size is more readily entangled. In the flow region, molecular entanglements will constrain translational motion such that the linear polymer has a higher zero-shear viscosity. In contrast, branches of appreciable length or sparse branching can lead to considerably more entanglements and act as permanent constraints that prevent translational motion. A polymer with such branching will have a higher zero-shear viscosity compared to its linear analog. When the branches are large enough to cause more entanglements, the flow region, where uncoupling begins, will shift to longer times or lower frequencies (shear rates). The explanation is that longer times are needed for the coordinated motions of uncoupling to take place. When the branches are not sufficiently long enough to increase the number of entanglements, slippage occurs at much shorter times or higher frequencies (shear rates). In the first situation, the zero-shear viscosity of the branched polymer will be reached at a lower shear rate compared to the corresponding linear polymer, while for the latter case, the Newtonian region will be reached at higher shear rates.

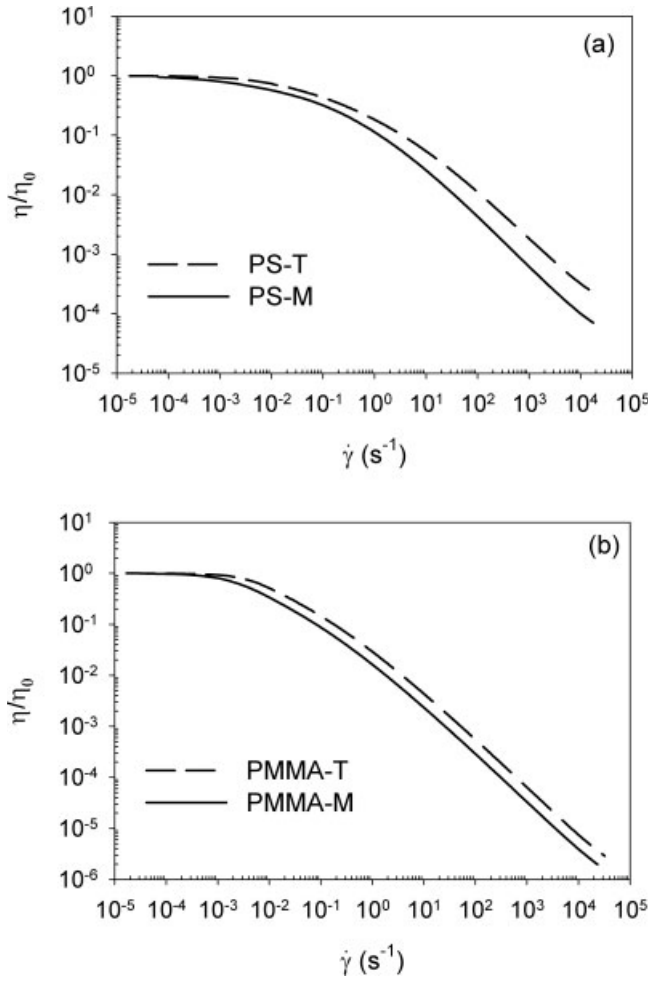

Figure 16 Reduced viscosity as a function of shear rate for polystyrene and poly(methyl methacrylate) samples.

CONCLUSIONS

PS and PMMA samples produced by free-radical polymerization with either a tetrafunctional (PS-T and PMMA-T) or monofunctional (PS-M and PMMA-M) initiator were characterized in detail by dilute solution and rheological methods. In the case of PS, SEC analysis with multiangle laser light scattering and viscometry revealed smaller radii of gyration and intrinsic viscosities for the sample produced with the tetrafunctional initiator. This reduction in molecular size confirmed that PS-T contained higher levels of branching than PS-M. In contrast, no differences were observed in R_g and $[\eta]$ plots for the comparison of PMMA samples.

Oscillatory shear experiments were performed at varying temperatures. The application of TTS was found to be valid for both sets of PS and PMMA samples. The WLF equation was found to fit the horizontal shift factors of the PS samples very well and a different set of parameter estimates were obtained for PS-T compared to PS-M. In the analysis of the PMMA data, an Arrhenius model provided a better fit compared to the WLF equation. Examination of the activation of viscous flow indicated that PMMA-T had a higher E_a value and the enhancement has been attributed to the presence of LCB. Activation energies for the PS samples were not determined to be statistically different. However, the Arrhenius model showed a clear lack of fit to the PS data, and thereby, resulted in larger confidence intervals for the PS activation estimates.

Viscoelastic functions measured during oscillatory shear experiments showed differences between the T and M samples due to branching (and in the case of PS, molecular weight and MWD). Dynamic data did not adequately reach the terminal region to calculate the zero-shear viscosity or steady-state recoverable compliance. As such, shear creep tests were performed. Lower values of the zero-shear viscosity were observed for the T samples and indicated the presence of branching. Differences in the steady-state recoverable compliance could not be attributed solely to the effect of branching because of polydispersity effects.

TABLE V
Summary: Evidence of Branching

Method	PS-T vs. PS-M	PMMA-T vs. PMMA-M
Solution properties		
SEC-MALLS-Visc (R_g, [η] plots)	Yes	No
Rheological properties		
E_a	Inconclusive	Yes
Dynamic data (G' and G'' vs. ω)	Inconclusive	Inconclusive
Shear creep data	Yes	Yes
η_0	Yes	Yes
J_e^0	Inconclusive	Inconclusive
Relaxation spectra	Yes	Yes
Viscosity–frequency data ($\|\eta\|^*$ vs. ω)	Yes	Yes
Overall	*Yes*	*Yes*

Using a rheological software package, creep time-dependent data were converted to frequency-dependent functions. Combined with the data collected from the oscillatory experiments, viscoelastic functions were extended over several decades. Relaxation spectra were determined from the combined data and indicated that the terminal region began at lower relaxation times for samples produced with the tetrafunctional initiator. The Cox-Merz rule was applied and the resulting viscosity-shear rate data were fit to a generalized Cross-Carreau model. PS-T and PMMA-T showed lower zero-shear viscosities, higher shear rates for the transition between the Newtonian and power-law region, and less shear thinning compared to PS-M and PMMA-M. All three observations are indications that the set of T samples are more branched than the M series.

In the end, it has been shown that samples produced with the tetrafunctional initiator are more branched than their counterparts produced with a monofunctional initiator. Table V provides a summary of the various methods examined in this study to detect evidence of branching. Fractionation along with the examination of dilute solution properties was found to be a less time and effort intensive method. The characterization by SEC-MALLS-Viscometry also required less material for testing compared to rheological methods. However, it was unable to detect the low levels of branching seen in PMMA-T that influenced the polymer's rheological behavior. The results obtained from viscoelastic data suggest that the branch lengths are not adequately long to increase the number of entanglements. This behavior is similar to that observed with low-density polyethylene.[52–54]

The authors thank ATOFINA Chemicals for providing samples of both Luperox JWEB50 and Luperox TBEC.

References

1. Staudinger, H.; Schulz, G. V. 1935, 68B, 2320.
2. Flory, P. J. J Am Chem Soc 1937, 59, 241.
3. Bywater, S. Adv Polym Sci 1979, 30, 89.
4. Roovers, J. Plast Eng 1999, 53, 285.
5. Burchard, W. Adv Polym Sci 1999, 143, 113.
6. Graessley, W. W. Acc Chem Res 1977, 10, 332.
7. Watanabe, H. Prog Polym Sci 1999, 24, 1253.
8. Small, P. A. Adv Polym Sci 1975, 18, 1.
9. Roovers, J. In Encyclopedia of Polymer Science and Engineering; Wiley: Toronto, 1983; Chapter 2.
10. Shiga, S. Polym Plast Tech Eng 1989, 28, 17.
11. Rudin, A. In Modern Methods of Polymer Characterization; Wiley: Toronto, 1991; Chapter 3.
12. Vega, J.; Aguilar, M.; Peon, J.; Pastor, D.; Martinez-Salazar, J. e-Polymers 2002, 46, 1.
13. Yu, Y.; DesLauriers, P. J.; Rohling, D. C. Polymer 2005, 46, 5165.
14. Janzen, J.; Colby, R. H. J Mol Struct 1999, 485/486, 569.
15. Jackson, C.; Chen, Y.-J.; Mays, J. W. J Appl Polym Sci 1996, 59, 179.
16. Shroff, R.; Mavridis, H. J Appl Polym Sci 1995, 57, 1605.
17. Shroff, R. N.; Mavridis, H. Macromolecules 1999, 32, 8454.
18. Wood-Adams, P.; Dealy, J. M.; deGroot, A. W.; Redwine, O. D. Macromolecules 2000, 33, 7489.
19. Trinkle, S.; Walter, P.; Friedrich, C. Rheol Acta 2002, 41, 103.
20. Wood-Adams, P.; Costeux, S. Macromolecules 2001, 34, 6281.
21. Wood-Adams, P. M.; Dealy, J. M. Macromolecules 2000, 33, 7481.
22. Kasehagen, L. J.; Macosko, C. W. J Rheol 1998, 42, 1303.
23. Kasehagen, L. J.; Macosko, C. W. J Rheol 1996, 40, 689.
24. Fityani-Trimm, S.; Dhib, R.; Penlidis, A. Macromol Chem Phys 2003, 204, 436.
25. Scorah, M. J.; Dhib, R.; Penlidis, A. J Polym Sci, Part A: Polym Chem 2004, 42, 5647.
26. Scorah, M. J.; Dhib, R.; Penlidis, A. J Macromol Sci, Part A: Pure Appl Chem 2005, 42, 403.
27. Podzimek, S. J Appl Polym Sci 1994, 54, 91.
28. Gabriel, C.; Münstedt, H. Rheol Acta 1999, 38, 393.
29. Zimm, B. H.; Stockmayer, W. H. J Chem Phys 1949, 17, 1301.
30. Burchard, W. Macromolecules 1974, 7, 841.
31. Casassa, E. F.; Berry, G. C. J Polym Sci, Part A-1: Polym Chem 1966, 4, 881.
32. Terao, K.; Mays, J. W. Eur Polym J 2004, 40, 1623.
33. Fetters, L. J.; Hadjichristidis, N.; Lindner, J.S.; Mays, J. W. J Phys Chem Ref Data 1994, 23, 619.
34. Gabriel, C.; Münstedt, H. Rheol Acta 2002, 41, 232.
35. Foster, G. N.; Hamielec, A. E.; MacRury, T. B. ACS Symp Ser 1980, 138, 131.
36. Grinshpun, V.; Rudin, A.; Russell, K. E.; Scammell, M. V. J Polym Sci, Part B: Polym Phys 1986, 24, 1171.
37. Brandrup, J.; Immergut, E. H.; Grulke, E. A. Polymer Handbook; Wiley: New York, 1999.
38. Mavridis, H.; Shroff, R. N. Polym Eng Sci 1992, 32. 1778.
39. Ferry, J. D. Viscoelastic Properties of Polymers; Wiley: Toronto, 1980.
40. Scorah, M. J. Ph.D. Thesis, Department of Chemical Engineering, University of Waterloo, Waterloo, ON, Canada, 2005.
41. Rouse, P. E. J Chem Phys 1953, 21, 1272.
42. Carella, J. M.; Graessley, W. W.; Fetters, L. J. Macromolecules 1984, 17, 2775.
43. Mcneill, I. C.; Zulfiqar, M.; Kousar, T. Polym Degrad Stab 1990, 28, 131.

44. Kashiwagi, T.; Inaba, A.; Brown, J. E.; Hatada, K.; Kitayama, T.; Masuda, E. Macromolecules 1986, 19, 2160.
45. Nising, P.; Zeilmann, T.; Meyer, T. Chem Eng Technol 2003, 26, 599.
46. Dealy, J.; Wissbrun, K. F. Melt Rheology and its Role in Plastics Processing; Van Nostrand Reinhold: New York, 1989.
47. Weese, J. Comput Phys Commun 1993, 77, 429.
48. Honerkamp, J.; Weese, J. Rheol Acta 1993, 32, 65, .
49. Fuchs, K.; Friedrich, C.; Weese, J. Macromolecules 1996, 29, 5893.
50. Cox, W. P.; Merz, E. H. J Polym Sci 1958, 28, 619.
51. Wood-Adams, P. J Rheol 2001, 45, 203.
52. Mendelson, R. A.; Bowles, W. A.; Finger, F. L. J Polym Sci, Part A-2: Polym Phys 1970, 8, 127.
53. Chartoff, R. P.; Maxwell, B. J Polym Sci, Part A-2: Polym Phys 1970, 8, 455.
54. Doerpinghaus, P. J.; Baird, D. G. J Rheol 2003, 47, 717.